Applied Mathematical Modelling 104 (2022) 1–20

Contents lists available at ScienceDirect

Applied Mathematical Modelling

journal homepage: www.elsevier.com/locate/apm

Fire-spotting generated fires. Part II: The role of flame geometry and slope

Vera N. Egorova [a,*], Andrea Trucchia [b], Gianni Pagnini [c,d]

[a] Departamento de Matemática Aplicada y Ciencias de la Computación, E.T.S.I. Industriales y de Telecomunicación, Universidad de Cantabria, E-Santander 39005, Spain
[b] CIMA Research Foundation, Via Armando Magliotto 2, Savona I-17100, Italia
[c] BCAM–Basque Center for Applied Mathematics, Alameda de Mazarredo 14, Bilbao E-48009, Basque Country, Spain
[d] Ikerbasque–Basque Foundation for Science, Plaza Euskadi 5, Bilbao E-48009, Basque Country, Spain

ARTICLE INFO

Article history:
Received 15 April 2021
Revised 20 October 2021
Accepted 7 November 2021
Available online 17 November 2021

Keywords:
Wildfire
Fire-spotting
Flame length
Fireline intensity
Terrain slope
Rothermel model

ABSTRACT

This is the second part of a series of two papers concerning fire-spotting generated fires. While, in the first part, we focus on the impact of macro-scale factors on the growth of the burning area by considering the atmospheric stability conditions, in the present study we focus on the impact of meso-scale factors by considering the effects of the flame geometry and terrain slope. First, we discuss the phenomenological power law that relates flame length and fireline intensity by reporting literature data, analysing a formula originally proposed by Albini, and deriving an alternative formula based on the energy conservation principle. Subsequently, we extend the physical fire-spotting parametrisation `RandomFront` adopted in the first part by including flame geometry and slope. Numerical examples show that fire-spotting is affected by flame geometry and, therefore, cannot be neglected in simplified fire-spread models used in operational software codes for wildfire propagation. Meanwhile, we observe that terrain slope enhances the spread of a fire at a higher rate than the augmentation of fire-spotting generated fires, such that a rapid merging occurs among independent fires.

1. Introduction

Fire-spotting is a feature of forest fires that, more than others, manifests in the extension in the space of wild burning events. Fire-spotting, as a part of wildfire systems, is a challenging, multiscale, physical problem in itself, because it includes processes that range from chemical to meteorological scales [1].

Indeed, fire-spotting starts by generating firebrands at the meso-scopic scale of a flame's geometry; at the micro-scopic scale it involves chemical reactions that enable firebrands to ignite a new fire, while at the macro-scopic scale it is driven by the boundary-layer meteorology, which is responsible for the rising and transportation of firebrands.

In this second part of our series of two papers concerning fire-spotting generated fires, we focus on the role of the meso-scopic characteristics of wildfires. We refer, in particular, to flame geometry, which strongly affects fire spreading [2], and to

* Corresponding author.
E-mail address: vera.egorova@unican.es (V.N. Egorova).

https://doi.org/10.1016/j.apm.2021.11.010

Nomenclature

C_d	Drag coefficient, $C_d = 0.45$
c_p	Specific heat of fuel, $c_p = 1121.0$ kJ kg^{-1} K^{-1}
D	Diffusion coefficient (m^2 s^{-1})
e	Internal energy of gas (J)
g	Gravitational acceleration, $g = 9.81$ m s^{-2}
Fr	Froude number
H	Mechanical energy (J)
H_{max}	Maximum loftable height (m)
h	Flame height (m)
I_f	Fireline intensity (Wm^{-1})
L_f	Flame length (m)
ℓ	Firebrand landing distance (m)
ℓ_{max}	Maximum travel distance (m)
$\dot{m}$	Mass flow rate of flame fluid (kg s^{-1})
P	Pressure (kg m^{-1} s^{-2})
P_f	Energy flow rate in convection column above a line of fire (J s^{-1})
P_w	Energy flow rate in wind field (J s^{-1})
Q	Heat transformed into gas (J)
$q(\ell)$	Firebrand landing distribution
R	Fuel consumed per unit area in active flaming front (kg m^{-2})
r	Firebrand radius (m)
R_a	Gas constant per unit mass of air (J kg^{-1} K)
T	Flame temperature (K)
T_a	Ambient air temperature (K)
U	Mean wind velocity (m s^{-1})
V	Volume (m^3)
$V_{ROS}(\mathbf{x}, t)$	rate of spread (m s^{-1})
W	Work done on gas (J)
W_{sh}	Shaft work used to move the fluid (J)
w	Vertical velocity (m s^{-1})
w_c	Characteristic buoyant velocity (m s^{-1})
w_f	Vertical component of flame velocity (m s^{-1})
z	Altitude (m)
z_p	p-th percentile, $z_p = 0.45$
α	Entrainment constant
β	Packing ratio, β =(overdry bulk density)/(ovendry particle density)
β_{op}	Optimum packing ratio
β_0	Pre-factor of the flame length – fireline intensity interdependence
β_1	Exponent of the flame length – fireline intensity interdependence, $\beta_1 = 2/3$
β_2	Correction factor in (52), $\beta_2 = 0.7$
β_3	Correction factor in (56), $\beta_3 = 0.945$
Δ	Horizontal cross-sectional sheet of the flame (m^2)
ε	Kinetic energy dissipation (m^2 s^{-3})
η	Fraction of impinging air stream
θ	Flame angle (rad)
ω	Slope angle (rad)
κ	Byram's energy criterion, $\kappa = P_f/P_w$
μ	Median of the lognormal distribution $q(\ell)$
ρ	Ambient air mass density, $\rho = 1.1$ kg m^{-3}
ρ_f	Density of the wildland fuels, $\rho_f = 542$ kg m^{-3}
ρ_{fm}	Flame mass density (kg m^{-3})
σ	Parameter of lognormal distribution $q(\ell)$
ϕ_{slope}	Slope correction in Rothermel's ROS model
ϕ_{wind}	Wind correction in Rothermel's ROS model
φ	Net low heat of combustion (kJ kg^{-1})

Fig. 1. Flame geometry of real wildland fire in flat terrain.

terrain slope. Additionally, an accurate estimation of geometrical properties allows a determination of how wildfires can be controlled: indeed, flame length is used to determine the size of fire control lines [3], while flame height is used to predict the heat flux exposure [4].

Establishing indicators for the onset of erratic or unexpected wildfire behaviour is an important endeavour, while flame characteristics are fundamental features for the determination of combustion regimes [5]. Moreover, flame geometry is a descriptor of the surrounding vegetation; therefore, it is considered in fire-fighting strategies [6]. Another valuable quantity for characterising fires is fireline intensity, which is used by practitioners to predict the probability of house survival during bush fires [7]; it is linked with stem-bark char height and crown scorch height, which are important descriptors of surface fire behaviour and useful for studying post-fire impacts [8].

Since the introduction of Byrams formula [9], several empirical laws have been proposed for the interdependency between flame geometry, in terms of flame length, and fireline intensity [8]. Usually, these laws are established empirically, using statistical methods for quantitatively fixing the value of the involved parameters, which, unfortunately, results in case-dependent values. Only a few attempts have been made to develop a physical model. The first was by Albini in 1981 [10], which was improved on by Nelson Jr. and co-authors, in 2012, by including entrainment [5]. A further approach was proposed by Marcelli et al. [11] based on radiative flux, with flame height defined as the height of the equivalent radiant panel. Another model, based on radiation, considers moisture content and energy losses, and was proposed by Ferragut and collaborators [12]. The relationships between flame geometry and the Froude number, or convection number, have also been studied [13–16], including their experimental approbation [17–19].

Therefore, motivated by the lack of this important foundation, we theoretically establish a formula for estimating the flame height and length in wildfires from the fireline intensity. The derivation is based on the energy conservation principle and on the concept of the energy flow rate in the convection column above a fireline, the latter was originally introduced by Byram in 1959 [20].

Evidently, flame geometry is strongly affected by wind (see Fig. 1) and terrain slope. In our formulation, we assume that, in the no-wind no-slope condition, flame geometry is fully characterised by the process's energy, while the wind and slope rule the flame tilting angle and they cause a stretching of the flame.

The actual impacts of wind and the slope on flame geometry are considered by combining the Byram relation between fireline intensity and the rate of spread (ROS) by using Rothermel's ROS model, which explicitly displays wind and slope corrections [21,22]. It turns out that the impacts of wind and slope on flame geometry depend on the same wind- and slope-correcting factors of the ROS: the flame length increases when they augment the ROS.

To conclude, fireline intensity is related to the propagation of a front and drives fire-spotting, which accelerates the spreading of a fire [23,24]; therefore, fire-spotting is crucial for simulating the evolution of a burning area, and cannot be disregarded. Due to its unpredictable nature, fire-spotting modelling, here, is considered through a statistical approach embodied in a proper probability density function (PDF). Wang [25] studied the downwind distribution of firebrands by considering the maximum travel distance, which also depends on the geometrical characteristics of a flame. Martin & Hillen [24] studied, in detail, the spotting distribution by considering launching and landing distributions. Kaur & Pagnini [26] proposed a physical parametrisation of the fire-spotting distribution by considering the maximum loftable height of a firebrand, mean wind, and fireline intensity.

Therefore, to estimate the impact of meso-scale factors on fire-spotting and wildfire propagation, we include flame geometry and slope in a physical parametrisation called `RandomFront` model, which has already been proposed and updated by this research group [27–30] as well as implemented in real cases [31], and adopted in Part 1 [32]. Within this parametrisation, numerical simulations show that flame geometry, particularly flame length, contributes to the generation of independent secondary fires. Meanwhile, terrain slope enhances the propagation of a front, such that independent secondary fires are rapidly merged.

As a final introductory remark, we clarify that some of the contents of this paper have already been presented in a preliminary version [33]. However, we emphasise that those common parts have indeed largely been revised and corrected for

the present paper; moreover, the current study includes an extension to cases with terrain slope, such that new numerical simulations have been executed from a different planning perspective.

The remainder of the paper is organised as follows. Section 2 is devoted to discussing the role of reduced-scale facilities in understanding and modelling full-scale wildfires, while Section 3 reports on the relation between flame length and fireline intensity. Section 4 deals with the derivation and analysis of Albini's formula relating flame length and fireline intensity. In Section 5, a new formula for such a relation is derived based on the energy conservation principle. The inclusion of this last formula in the fire-spotting `RandomFront` model is discussed in Section 6, while the corresponding simulations are reported in Section 7. Section 8, with final remarks, concludes.

2. Reduced-scale facilities and fire spreading models

It is well-known and has certainly been established that "small-scale flame dynamics provide limited insight into wildfire behavior" [34]. Many processes occur contemporarily during a wildfire event (e.g. buoyancy, convection, radiation, chemical reactions, and wind flow), spanning over so many ranges of temporal and spatial scales that they cannot scale simultaneously to allow for the derivation of simplified analogues [35].

Specifically, when dimensional analysis is strictly applied to forest fires, the non-dimensional quantities obtained can exceed 30 [36] or much more [37]; furthermore, when suitable sub-ensembles are selected on a physical basis, they account for 14 of such non-dimensional quantities [38], 11 [36,39], or at least 7 [40]. Then, despite this effort, a complete scaling that satisfies all the derived scaling laws is not possible.

This means that, within this framework, the formulation of a partial model is a unique viable option, which is more an art than a science, notwithstanding some physical reductionistic assumptions [36–38,41]. Only a few scaling laws have emerged as useful for a better understanding of fires; however, regrettably, these scaling laws concern different combustion phenomena [38,40,42–47].

Even worse, besides convection, radiative heat transfer is the other heat transfer mechanism responsible for fire spread; however, radiation effects do not scale [38,43] because their importance increases with increasing flame size [43,48]. The relative contribution of convective and radiative heating rates depends on the fuel and the environment [49]; therefore, a similarity analysis is not reliable for studying fire spread, because a change of the main heat transfer mechanism, i.e. from convective to radiative or vice versa, may occur [43,45,49]; (see, also, [50] and the references therein).

Therefore, the identification of a heat transfer mechanism also requires an investigation of the fuel bed in which the fire spreads, while in reduced-scale facilities, such fuel beds should be as similar as possible to those of the full-scale events [34,43]. Indeed, when reduced-scale fuel beds do not replicate the natural fuel-complex structure of the full-scale wildfire, the interpretation of the flammability trials cannot be extrapolated beyond the experimental setting [51]: this occurs, for example, with crown fires, whose scaling fails because bench-scale tests are mainly based on radiation heat flux [52]. Moreover, the moisture content does not scale, because its equilibrium state depends on ambient conditions [53], and it transpires that even the ROS does not scale when the fire spreads in steep-slopes or high wind-speed conditions [53].

Moreover, reduced-scale experiments are generally unreliable in cases with important wind-fire interactions, because of the difficulties in reproducing atmospheric stability, except when it is neutral [43]; additionally, the unreliability applies in cases with multiple fire interactions, because the latter depends on the wind that is generated by the fires themselves [43]. Hence, generally, reduced-scale experiments are unlikely to contribute to an understanding of wildfires; for a discussion, see, for example, [34,53–55].

Finally, with respect to the present research - where the role of flame geometry is investigated in fire-spotting generated fires - it is reported that, since radiative effects do not scale [38,43], and due to the strong relation between radiative heat transfer and flame geometry [11,12,43,48,56], the modelling approach discussed here cannot be based on or obtain input from studies concerning pool fires, e.g. [42]; neither can cases with wind flow be useful, e.g. [47,57], because they do not provide any understanding of the flame geometry and entrainment rate in real wildfires. Indeed, in pool fires, the fuel-fire and wind-fire interactions occur with parallel fuel flow and buoyancy, unlike in wildfires, where wind and buoyancy are in perpendicular directions [45]; furthermore, generally, a poor understanding of wildfires from pool fires emerges already at the level at which the fire spreads because a different setting of the Strouhal–Froude numbers is necessary for displaying correlation: the burner diameter-length scale is replaced in wildfires by the flame length rather than by the horizontal flame zone depth [45].

3. Flame geometry and fireline intensity: what the data say

A flame is geometrically characterised by height, length, and tilt. Different definitions are found in the literature, e.g. [17,58,59]; however, all the existing definitions are linked by trigonometric formulae. In this study, we adopt, for our convenience, definitions that allow for stressing the separation between flame angle and terrain slope angle [56,59–61]. We define flame geometry as follows:

Definition 1 (Flame height)**.** The flame height, h (m), is measured along the axis perpendicular to the terrain that can be sloped.

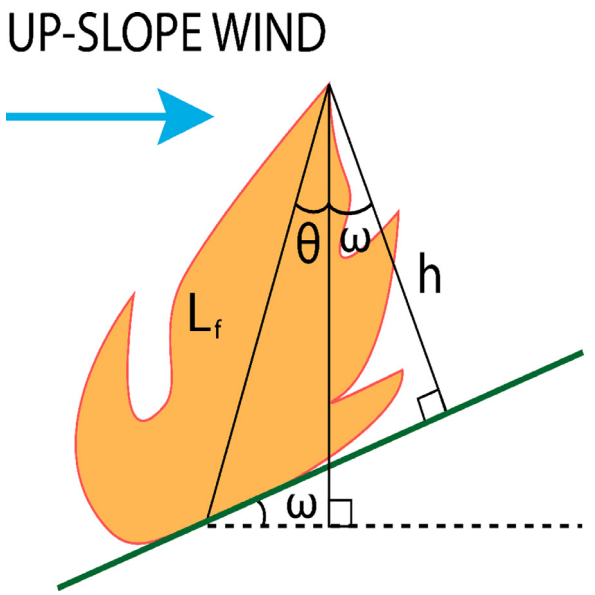

Fig. 2. Flame geometry in cases of up-slope wind such that $h = L_f \cos(\theta + \omega)$.

Definition 2 (Flame length)**.** The flame length L_f (m) is defined as the distance between the flame height tip and the mid-point of the flame depth [17,58,59].

Definition 3 (Flame tilt)**.** The flame tilt is defined as the sum of the terrain slope angle ω and the tilting angle θ.

These flame geometry characteristics are related by the formula, $h = L_f \cos(\theta + \omega)$ (see Fig. 2).

The tilting angle θ accounts for the concurrent effects of wind and slope that are not joined in a simple additive formula, i.e. $\theta = \theta(U, \omega) \neq \theta(c_U U + c_\omega \omega)$ where U is the mean wind while the parameters c_U and c_ω represent the corresponding dimensional scales; and it reduces to the corresponding angle in the limiting cases:

$$\theta = \theta(U,\omega) = \begin{cases} \theta(U,0) = \theta_w(U)\,, & \textit{with wind but no–slope}\,, \\ \theta(U,\omega)\,, & \textit{with slope and wind}\,, \\ \theta(0,\omega) = \theta_s(\omega)\,, & \textit{with slope but no–wind}. \end{cases} \tag{1}$$

Several experimental measurements display a power-law relationship between the flame length L_f and the fireline intensity I_f. The fireline intensity I_f (kW m^{-1}), was established by Byram [9,62,63] from measurements of fire spread and fuel consumption. Notwithstanding, fireline intensity is of paramount importance in quantifying wildfire behaviour, both in applied and in theoretical studies (see, e.g. [8,27,64,65]); its experimental measurements remain an issue [66]. Fireline intensity is also related to flame geometry (see [58,62] and the references therein). A widely used approximated empirical relation is given by [8,17]

$$L_f = \beta_0 I_f^{\beta_1}\,, \tag{2}$$

where β_0 and β_1 are two positive parameters. Unfortunately, the values of β_0 and β_1 tend to be mostly scattered, while the sole constraint that emerges is that the power-law exponent is $0 < \beta_1 < 1$ (see Table 1 for a list from the literature and Fig. 3 for their graphical representation). Thus, a theoretical determination of the parameters β_0 and β_1 is necessary to provide an insight into reducing and clarifying such variability.

In the following section, first, we report and discuss the estimation of the flame height derived by Albini [10], which is based on the vertical variation of the mass flow rate of the flame fluid. We also consider the improvements to Albini's formula by Nelson Jr. and co-authors [5], who, by considering the characteristic buoyant velocity, obtained $\beta_1 = 2/3$. Later, we also derive and discuss an estimation based on the energy conservation principle that leads to $\beta_1 = 2/3$.

4. The vertical variation of the mass flow rate of the flame fluid for estimating the flame height: Albini's formula

To the best of our knowledge, the first model in the literature for a wind-blown turbulent flame from a line fire was proposed by Albini in 1981 [10]. Albini's derivation, which is intended for a case with wind and flat terrain, i.e. $\omega = 0$, is based on the mass flow rate of the flame fluid, here denoted by $\dot{m}$ (kg s^{-1}), which is defined at the altitude z as $\dot{m} = \rho_{fm} w_f \Delta$, where ρ_{fm} (kg m^{-3}), w_f (m s^{-1}), and Δ (m^2) are the flame mass density, the vertical component of flame velocity, and the horizontal cross-sectional sheet of the flame, respectively. The horizontal wind generates a change in the mass flow rate at

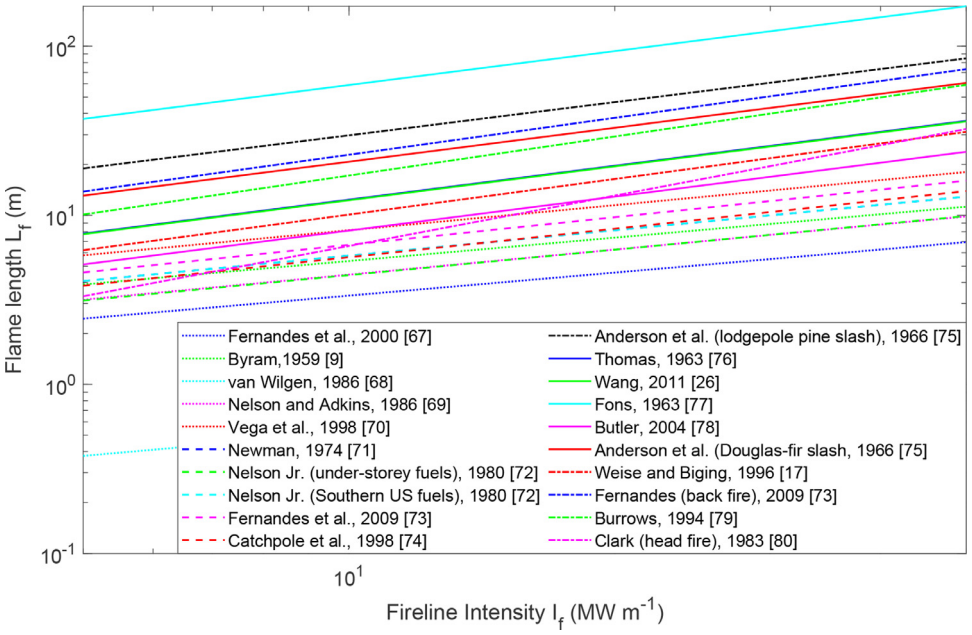

Fig. 3. Flame length–fireline intensity dependencies from Table 1.

Table 1
Empirical parameters of the flame length–fireline intensity interdependence according to formula (2).

References	β_0	β_1
Fernandes et al., 2000 [67]	0.0516	0.453
Byram, 1959 [9]	0.0775	0.46
van Wilgen, 1986 [68]	0.0075	0.46
Nelson Jr. and Adkins, 1986 [69]	0.0475	0.493
Vega et al., 1998 [70]	0.087	0.493
Newman, 1974 [71]	0.0577	0.5
Nelson Jr. (under-storey fuels), 1980 [72]	0.04425	0.5
Nelson Jr. (Southern US fuels), 1980 [72]	0.0577	0.5
Fernandes et al. (head fire), 2009 [73]	0.045	0.543
Catchpole et al., 1998 [74]	0.0325	0.56
Anderson et al. (lodgepole pine slash), 1966 [75]	0.074	0.651
Thomas, 1963 [76]	0.02665	2/3
Wang, 2011 [25]	0.026445	2/3
Fons, 1963 [77]	0.127	2/3
Butler, 2004 [78]	0.0175	2/3
Anderson et al. (Douglas-fir slash), 1966 [75]	0.0447	2/3
Weise and Biging, 1996 [17]	0.016	0.7
Fernandes (back fire), 2009 [73]	0.029	0.724
Burrows, 1994 [79]	0.0147	0.767
Clark (head fire), 1983 [80]	0.000722	0.99

two different altitudes, while this change results in the equation

$$\frac{d\dot{m}}{dz} = \eta\,\rho U\,, \tag{3}$$

where η is a constant fraction of impinging air stream incorporated into the flame fluid flow; ρ (kg m^{-3}) and U (m s^{-1}) are the characteristic air density and the mean wind speed at a height z, respectively.

Denoting the flame height by h (m), and assuming that ρU is constant in the interval $0 \le z \le h$, then, after the integration of (3) over z in the same interval $0 \le z \le h$, we have

$$\dot{m}_{\rm t} = \dot{m}_{\rm g} + \eta\,\rho U\,h, \tag{4}$$

where $\dot{m}_{\rm t}$ and $\dot{m}_{\rm g}$ refer to the measurement at the flame top $z = h$ and at the ground level $z = 0$, respectively.

The mass flow rate of the flame fluid $\dot{m}$ is related to the flame temperature T (K) by the sensible energy conservation formula [5]

$$\frac{d(\dot{m}c_{\rm p}T)}{dz} = c_{\rm p}T_{\rm a}\frac{d\dot{m}}{dz}, \tag{5}$$

where c_p (kJ kg^{-1} K^{-1}) is the specific heat of air at constant pressure and T_a (K) is the free-air temperature at the elevation of the fire (absolute ambient air temperature), such that, after the integration over z, it leads to

$$\frac{\dot{m}_t}{\dot{m}_g} = \frac{T_g - T_a}{T_t - T_a}, \tag{6}$$

where T_t and T_g refer to the measurement at the flame top $z = h$ and at the ground level $z = 0$, respectively. Finally, by combining (4) and (6), flame height can be obtained as

$$h = \frac{(\dot{m}_t - \dot{m}_g)}{\eta\,\rho U} = \frac{T_g - T_t}{T_t - T_a}\frac{\dot{m}_g}{\eta\,\rho U} = h_{A81}. \tag{7}$$

In 2012, Nelson Jr. and co-authors [5] followed the same formulation by Albini; however, they also introduced the fireline intensity I_f through the formula

$$I_f = \dot{m}_g c_p (T_g - T_a). \tag{8}$$

By plugging Formula (8) into (7), Albini's formula leads to a linear relation between the fireline intensity and the flame height, i.e.

$$h = \frac{(T_g - T_t)}{(T_t - T_a)(T_g - T_a)}\frac{I_f}{\rho c_p \eta U}. \tag{9}$$

Moreover, Nelson Jr. and co-authors considered, in addition, an estimation of entrainment: the mixing between the mass flow rate and the ambient air. By using the characteristic buoyant velocity w_c and by inferring

$$\eta U = \alpha w_c = \alpha\left(\frac{2gI_f}{\rho c_p T_a}\right)^{1/3}, \tag{10}$$

where g (m s^{-2}) is the acceleration due to gravity and α is an entrainment constant, the formula for computing the flame height takes the form

$$h = \frac{T_a(T_g - T_t)}{\alpha(T_t - T_a)(T_g - T_a)}\left[\frac{1}{2g(\rho c_p T_a)^2}\right]^{1/3} I_f^{2/3} = h_{N12}. \tag{11}$$

The factor $(T_g - T_t)/(T_t - T_a)$ in (11) is stated equal to 1 by Nelson Jr. and co-authors [5]; however, this does not always hold.

Summarising, the flame height originally derived using this approach turns out to be linearly proportional to the fireline intensity, i.e. $h \sim I_f$. However, in the following revised formulation by Nelson Jr. and co-authors [5], by formulating flame characteristic equations and considering the entrainment for low-wind fires [5], the flame height is found to be proportional to the fireline intensity with the power 2/3.

Remark 1. From Albini's original derivation with a flat terrain, by taking $h \sim I_f$, after some manipulations that are not reported here (see [10, p. 164, formulae (36–39)]), the flame length for the minimum wind speed turns out to be proportional to the fireline intensity to the power 2/3, i.e. $L_f \sim I_f^{2/3}$: this means that the flame tilt turns out to be dependent on the fireline intensity, i.e. $\cos\theta \sim I_f^{1/3}$.

Remark 2. From the revised derivation of Albini's formula by Nelson Jr. and co-authors [5], with a flat terrain, it follows that $h \sim I_f^{2/3}$, and, after some manipulations not reported here (see [5, p. 131, formulae (18–24)]), the flame tilting angle θ turns out to be independent of the fireline intensity, which means that the flame length is proportional to the power 2/3, i.e. $L_f \sim I_f^{2/3}$.

Remark 3. The formalism developed by Albini [10], followed by Nelson Jr. and co-authors [5], holds when the vertical variations in the pressure are negligible with respect to the temperature variations, while an in-canopy profile is considered for temperature and wind with relaxing factors of the same order.

Indeed, the derivation of Albini's formula is based on the assumption $\rho U = constant$ in the integration interval $0 \le z \le h$. However, although, for general purposes, ρ and U can be separately approximated as constant ambient air characteristics, the integration interval is indeed very small with respect to the length scales of the atmospheric boundary layer and, moreover, the process occurs inside a forest canopy. We have found that possible reasoning for supporting the assumption $\rho U = constant$, is the following. Temperature [81–83] and wind [84–86] profiles inside a canopy can be modelled by

$$T(z) = T_g + (T_{H_c} - T_g)\,e^{-a(1-z/H_c)}, \quad U(z) = U_{H_c}\,e^{-b(1-z/H_c)}, \tag{12}$$

where H_c is the top of the canopy, such that T_{H_c} and U_{H_c} are the temperature and wind values at $z = H_c$, respectively, while the parameters a and b are the relaxing factors. Then, using the ideal gas law, i.e. $P = \rho R_a T'$ (kg m^{-1} s^{-2}), where R_a (J kg^{-1} K) is the gas constant per unit mass of air, without loss of generality, we have applied the shift $T' = T - T_g$, such that $T'_{H_c} = T_{H_c} - T_g$, from the hydrostatic balance, i.e. $\frac{dP}{dz} + \rho g = 0$; thus, it follows that

$$P = P_0 \exp\left\{-\frac{g}{R_a T'_{H_c}}\int_0^z \frac{T'_{H_c}}{T'}\,d\xi\right\}, \tag{13}$$

where $g/(R_a T'_{H_c})$ establishes a very large length scale and, thus, $P \simeq P_0$ in $0 \leq z \leq H_c$. Finally, within this framework, again from the ideal gas law, we have that

$$\rho \simeq \frac{P_0}{R_a T'} = \frac{P_0}{R_a T'_{H_c}} e^{a(1-z/H_c)}, \tag{14}$$

which leads to the constant $\rho U \simeq P_0 U_{H_c}/(R_a T'_{H_c})$ when $a \simeq b$.

Remark 4. Albini's formula cannot account for terrain slope and requires entrainment.

Indeed, when a fire propagates over a sloped terrain, the flame height is geometrically affected by the slope angle ω according to the geometrical setting shown in Fig. 2. This modification is mainly because the flame height is driven by the buoyancy force. The direction of the wind and the ROS remain parallel to the terrain and directed in the up-slope direction, while the normal direction of the buoyant flux is independent of the terrain slope, such that, over a sloped terrain, it is not in the cross-slope direction.

By assuming the notation reported in Fig. 2, it is possible to show that Albini's formula (9) cannot account for the terrain slope, and that it calls for the inclusion of entrainment (11). Indeed, the derivation of Formula (9) begins with the normal variation of the mass flow rate that is proportional to the wind component in the perpendicular direction. Hence, let $\hat{z}$ be the normal direction determined by the buoyancy force; Formula (3) becomes

$$\frac{d\dot{m}}{d\hat{z}} = \eta \rho U \cos\omega, \tag{15}$$

where $U \cos\omega$ is the projection of the wind from the up-slope direction to the direction perpendicular to $\hat{z}$.

Under the same assumptions used for the derivation of (9), the integration of (15) yields

$$m_t = m_g + \eta \rho U \cos\omega \, h_{\hat{z}}, \tag{16}$$

such that, after using (6),

$$h_{\hat{z}} = \frac{T_g - T_t}{T_t - T_a} \frac{\dot{m}_g}{\eta \rho U \cos\omega} = \frac{h_{A81}}{\cos\omega}, \tag{17}$$

where h_{A81} is the flame height originally derived by Albini, defined in (7); finally, by noting that, in the present geometrical setting, $h = h_{\hat{z}} \cos\omega$, it follows that $h = h_{A81}$, which clearly does not account for the terrain slope.

In the adopted geometrical setting, the entrainment ratio (10) turns out to be

$$\eta U \cos\omega = \alpha w_c = \alpha \left(\frac{2 g I_f}{\rho c_p T_a} \right)^{1/3}; \tag{18}$$

then, using Formula (9), and remembering the flame height h_{N12} derived by Nelson Jr. and co-authors through the inclusion of entrainment (11), it holds that

$$h = \frac{1}{\alpha} \frac{T_a (T_g - T_t)}{(T_t - T_a)(T_g - T_a)} \left[\frac{1}{2g(\rho c_p T_a)^2} \right]^{1/3} I_f^{2/3} \cos\omega = h_{N12} \cos\omega, \tag{19}$$

which properly accounts for the terrain slope.

Remark 5. The derivation of the entrainment-including formula (11) is based on the *ad hoc* assumption (10), which connects the horizontal mean wind speed U and the characteristic vertical buoyant velocity w_c, which are indeed two independent quantities; this independence is reflected by the necessity to introduce two other independent parameters η and α. The horizontal and vertical components of the wind field are indeed related by turbulence in the form of the Reynolds stress tensor.

5. The energy conservation principle for estimating the flame height

5.1. Flame-height formula derivation

To improve the computation of the flame height, we set the theoretical underpinning for its estimation on the physical basis provided by the conservation of energy. We start by considering the paradigmatic case without wind and without slope, such that, from geometrical arguments, the flame height coincides with the flame length, while the energy balance is applied.

Our formulation assumes that the flame geometry is fully characterised by the energy process that provides the flame length in the no-wind no-slope case, while the wind and the slope affect the flame length through a geometrical rotation plus a stretching. The measured flame height is the elevation of the flame tip perpendicular to the ground.

We consider an air parcel located at the top of the flame, at the height $z = Z$ which is initially not buoyant, i.e. the vertical velocity w is equal to 0, while the parcel is heated by the flame. From the principle of conservation of energy, we have

$$e + PV + H - [e_0 + P_0 V_0 + H_0] = Q - W_{sh}, \tag{20}$$

where e (J) is the internal energy of the gas, P (kg m^{-1} s^{-2}) and V (m^3) are the pressure and the volume, respectively, H (J) is the mechanical energy, Q (J) is the heat transferred into the gas, while W_{sh} (J) is the shaft work used to move the fluid. The terms with the subscript 0 refer to the initial instant, while those without it refer to a generic instant. The initial mechanical energy is

$$H_0 = gZ, \tag{21}$$

which turns into

$$H = g\,(Z + \delta Z) + \frac{w^2}{2}, \tag{22}$$

where g is the acceleration due to gravity and δZ is the vertical displacement done by the air parcel. The work done on the gas is stated equal to the work necessary to balance the force of gravity, i.e.

$$W = PV - P_0V_0 + W_{sh} = -g\,(Z + \delta Z), \tag{23}$$

while the heat transferred into the gas is stated equal to the increase in the internal energy, i.e.

$$Q = e - e_0. \tag{24}$$

Plugging all the above formulae into (20), we obtain the vertical velocity due to the convection above the fireline as

$$|w| = \sqrt{2\ gZ}. \tag{25}$$

The conversion of turbulent kinetic energy into heat may also be included as a sink in (22), i.e. $H \to H - \varepsilon$ where ε is the turbulent kinetic energy dissipation, and also as a source in (24), i.e. $Q \to Q + \varepsilon$, and Formula (25) is still obtained.

To estimate the vertical velocity $|w|$ we now consider the energy flow rate in the convection column above a line of fire P_f, which is defined as the rate at which thermal energy is converted to kinetic energy in the convection column at a specified height z [20,87]. The equation is

$$P_f(z) = \frac{gI_f}{c_pT_a} = \frac{1}{2}\,\rho\,w^2|w| = \frac{1}{2}\,\rho\,|w|^3. \tag{26}$$

We assume that the definition of P_f given in (26) holds in the general case with wind and slope as well as in the case of a flat terrain with or without weak wind. We then distinguish between the two cases through the value of the fireline intensity, which is denoted by I_f in the general case and by I_{f_0} in the no-wind no-slope case. To establish the relation between the two values, we consider the linear relation between the ROS and the fireline intensity established by Byram's formula [9,62]. Later, we recast the fireline intensity by using the ROS from Rothermel's model [21,22], where an increasing factor due to wind and slope is employed. Rothermel's model is the most widely used in fire management systems and the wildfire theory. It is a surface-fire spread model based on the heat balance, and the ROS is computed by

$$V_{ROS} = V_{ROS_0}\left(1 + \phi_{wind} + \phi_{slope}\right), \tag{27}$$

where V_{ROS_0} (m s^{-1}) is the ROS in the no-wind no-slope case, while the coefficients ϕ_{wind} and ϕ_{slope} refer to the wind and slope effects. Hence, using Byram's classical formula [9,62] for both cases, i.e.

$$I_f = \varphi R V_{ROS}, \quad I_{f_0} = \varphi R V_{ROS_0}, \tag{28}$$

where φ (kJ kg^{-1}) is the fuel net low heat of combustion and R (kg m^{-2}) is the weight of fuel consumed per unit area in the active flaming front, from (27) and (28), we obtain

$$\frac{I_f}{I_{f_0}} = \frac{V_{ROS}}{V_{ROS_0}} = 1 + \phi_{wind} + \phi_{slope}, \tag{29}$$

where ϕ_{wind} and ϕ_{slope} are exactly those adopted for Rothermel's model, whose values are established as [21]

$$\phi_{wind} = CU^B\left(\beta/\beta_{op}\right)^{-E}, \quad \phi_{slope} = 5.275\,\beta^{-0.3}\tan^2\omega \tag{30}$$

with

$$C = 7.47\exp\left(-0.133\,\xi^{0.55}\right),$$
$$B = 0.02526\,\xi^{0.54},$$
$$E = 0.715\exp\left(-3.59\times10^{-4}\xi\right),$$

where $\xi = 4/d$ is the fuel particle surface-area-to-volume ratio, d is the diameter of circular particles or the edge length of square particles, β is the packing ratio defined as

$$\beta = \frac{\text{overdry bulk density}}{\text{ovendry particle density}}$$

and $\beta_{op} = 3.348\,\xi^{-0.8189}$ is the optimum packing ratio.

Finally, within this framework, by plugging (25) into (26), we have a formula in the no-wind no-slope case for computing the top of the flame Z. Since, in the energy balance procedure, we considered the case with negligible wind, from geometrical considerations, it follows that the flame is elongated by the rise Z of a flame parcel providing the flame length L_{f_0} and, due to the weak influence of wind, it is comparable to the flame height [76,88]; thus,

$$Z = L_{f_0} = \left[\frac{1}{2g(\rho c_p T_a)^2}\right]^{1/3} I_{f_0}^{2/3} = h_0, \tag{31}$$

where the subscript 0 stands for the absence of both wind and slope. Formula (31) straightforwardly follows from the application of the energy conservation principle and the concept of the energy flow rate in the convection column above a fireline.

When the wind is not negligible and the terrain is sloped, the estimation of the general-case flame length L_f is obtained from Formula (31) by replacing the fireline intensity I_{f_0} with its generalisation I_f given in (29), which yields

$$L_f = \left[\frac{1}{2g(\rho c_p T_a)^2}\right]^{1/3} I_{f_0}^{2/3}(1+\phi_{wind}+\phi_{slope})^{2/3} = \left[\frac{1}{2g(\rho c_p T_a)^2}\right]^{1/3} I_f^{2/3}. \tag{32}$$

From the ratio between (32) and (31), it follows that

$$\frac{L_f}{L_{f_0}} = (1+\phi_{wind}+\phi_{slope})^{2/3} \tag{33}$$

and, by combining 29–(32), it holds that

$$I_f = \sqrt{2g}\,\rho c_p T_a L_{f_0}^{3/2}(1+\phi_{wind}+\phi_{slope}). \tag{34}$$

Finally, from trigonometric reasons (see Fig. 2) and Formulae (31,33), it holds that

$$h = L_f\cos(\theta+\omega) = h_0\,(1+\phi_{wind}+\phi_{slope})^{2/3}\cos(\theta+\omega). \tag{35}$$

From formula (35), it turns out that, within the proposed derivation, conservation of energy provides the elongation of the flame in the basic case without wind and a flat terrain, while this elongation is stretched further by the wind and/or by the slope through the perturbation parameters ϕ_{wind} and ϕ_{slope}. Finally, wind and slope also affect the flame height through the geometrical effects embodied by the angles θ and ω.

Concerning the comparison with data, we observe that the 2/3 power law in the fireline intensity is consistent with the estimation by dimensional reasons as well as with previous empirical and theoretical results [8,10,19] (see, also, Table 1). Then, from comparing (31) and (2), it follows that $\beta_1 = 2/3$ and the pre-factor β_0 is

$$\beta_0 = \left[\frac{1}{2g(\rho c_p T_a)^2}\right]^{1/3}. \tag{36}$$

5.2. The role of the wind

Using (26) and (32), Formula (35) can be re-written as

$$h = \cos(\theta+\omega)\left[\frac{1}{2\,g^3\rho^2}\right]^{1/3} P_f^{2/3}, \tag{37}$$

where the horizontal energy flow also affects the flame height through the flame angle θ.

Byram introduced the concept of energy flow rate in the convection column above a fireline, as well as that of energy flow rate in the wind field [20,87]. The energy flow rate in the wind field P_w, is the rate of flow of kinetic energy through a vertical plane of unit area in a neutrally stable atmosphere at the height z specified for P_f, i.e.

$$P_w(z) = \frac{1}{2}\rho\,(U-V_{ROS})^2|U-V_{ROS}| = \frac{1}{2}\rho\,|U-V_{ROS}|^3. \tag{38}$$

Byram proposed to use the ratio $\kappa = P_f/P_w$ to characterise wildfires; thus, this ratio is also called Byram's energy criterion [20,87]. Byram pointed out that this ratio could be useful in understanding and predicting the onset of erratic fire behaviour and the occurrence of blow-up fires. In particular, a strong relationship has been observed between the occurrence of blow-up fires and values of this ratio close to 1 [89]. When this ratio is close to 1, the horizontal and vertical forcing are balanced, and the propagation is then not mainly driven by one or other forcing. In this situation, fluctuations govern the motion, and erratic behaviour follows. The ratio κ can be related to the so-called convective Froude number [89].

Let us consider Byram's energy criterion; from (26) and (38), we have the following equalities:

$$\kappa = \frac{|w|^3}{|U-V_{ROS}|^3} = \frac{2\,gI_f}{\rho c_p T_a|U-V_{ROS}|^3}. \tag{39}$$

From the left side of Formula (39), it holds that

$$|w| = \kappa^{1/3}\,|U - V_{\mathrm{ROS}}|. \tag{40}$$

Entrainment can roughly be understood as the mix between the ambient air and the rising plume of hot air above the fireline. From this viewpoint, the ratio between the wind U and the quantity $|U - V_{\mathrm{ROS}}|$ states how much the horizontal mean wind enters into the rising column. Hence, we replace, here, the entrainment assumption (10) with the relation

$$\eta U = |U - V_{\mathrm{ROS}}|. \tag{41}$$

Using Formula (41), we have a number of results. Combining (40) and (26), from (41), we obtain

$$\eta U = |U - V_{\mathrm{ROS}}| = \frac{|w|}{\kappa^{1/3}} = \frac{1}{\kappa^{1/3}}\left(\frac{2\,gI_{\mathrm{f}}}{\rho c_{\mathrm{p}} T_{\mathrm{a}}}\right)^{1/3}, \tag{42}$$

which, compared with (10), yields

$$\alpha = \frac{1}{\kappa^{1/3}}. \tag{43}$$

Therefore, by comparing (19), (32), (35), and (43), it follows that

$$\cos(\theta + \omega) = \frac{T_{\mathrm{a}}(T_{\mathrm{g}} - T_{\mathrm{t}})}{(T_{\mathrm{t}} - T_{\mathrm{a}})(T_{\mathrm{g}} - T_{\mathrm{a}})}\,\kappa^{1/3}\cos\omega, \tag{44}$$

where the effect of the wind appears indirectly through the ambient temperature T_{a}, and, if κ is replaced by (40), then the angle θ increases when the wind increases.

Formula (44) establishes, for a given slope ω, a method of measuring the flame angle θ - which is a local geometric information that depends on the wind - in terms of the temperature and of the Byram ratio; these are indeed general characteristics of a fire and the environment, and thus an *effective* estimation of θ is provided. This ability to effectively estimate the angle θ turns out to be a useful property of formula (44), if is implemented in operational simulators of wildfires.

Concerning the flame height, from (44), Formula (35) becomes

$$h = \frac{T_{\mathrm{a}}(T_{\mathrm{g}} - T_{\mathrm{t}})}{(T_{\mathrm{t}} - T_{\mathrm{a}})(T_{\mathrm{g}} - T_{\mathrm{a}})}\,h_0(1 + \phi_{\mathrm{wind}} + \phi_{\mathrm{slope}})^{2/3}\,\kappa^{1/3}\cos\omega. \tag{45}$$

5.3. Analysis of ROS

The formulae derived in the previous sections can be manipulated to derive further formulae and, in particular, some useful relations. One such useful relation relates the ROS with the flame length. Indeed, using Formulae 28–(34), it holds that

$$V_{\mathrm{ROS}} = \frac{\rho c_{\mathrm{p}} T_{\mathrm{a}}}{\varphi R}\sqrt{2g}\,L_{\mathrm{f_0}}^{3/2}\left(1 + \phi_{\mathrm{wind}} + \phi_{\mathrm{slope}}\right) = \frac{\rho c_{\mathrm{p}} T_{\mathrm{a}}}{\varphi R}\sqrt{2g}\,L_{\mathrm{f}}^{3/2}, \tag{46}$$

which is consistent with the empirical data in Table 4-2 in [90], in the sense that increasing the flame length accelerates the fire spreading.

Moreover, within the theoretical framework that led to formula (35), the following remark can be made on the perturbation parameters ϕ_{wind} and ϕ_{slope} of Rothermel's model of the ROS.

Remark 6. From geometrical reasons, it follows that $h < h_0$; then, it holds that

$$\left(1 + \phi_{\mathrm{wind}} + \phi_{\mathrm{slope}}\right)^{2/3}\cos(\theta + \omega) < 1, \tag{47}$$

from which

$$\phi_{\mathrm{wind}} + \phi_{\mathrm{slope}} < [\cos(\theta + \omega)]^{-3/2} - 1, \tag{48}$$

and the upper bound of the tilting angle θ is

$$\theta < \arccos[(1 + \phi_{\mathrm{wind}} + \phi_{\mathrm{slope}})^{-2/3}] - \omega. \tag{49}$$

6. Application to the firebrand landing distribution

In anticipation of the study on the role of flame geometry and slope on fire-spotting generated fires, we consider RandomFront [29], a physical parameterisation of fire spotting for operational fire spread models, which was adopted in Part 1 [32]. Specifically, we consider the downwind firebrand landing distance ℓ to be distributed according to a lognormal $q(\ell)$ [26,28]:

$$q(\ell) = \frac{1}{\sqrt{2\pi}\,\sigma\,\ell}\exp\left\{-\frac{1}{2}\left[\frac{\ln(\ell/\mu)}{\sigma}\right]^2\right\}, \tag{50}$$

with a median μ and a mode $\mu e^{-\sigma^2}$, such that [26]

$$\mu = H_{\max}\left[\frac{3}{2}\frac{\rho}{\rho_f}C_d\right]^{1/2}, \tag{51}$$

where $H_{\max}$ is the maximum loftable height (m), ρ_f (kg m^{-3}) is the fuel density, and C_d is the drag coefficient. The maximum loftable height $H_{\max}$ depends on the fireline intensity and atmospheric stability [26,91]; a detailed study of this dependence and the impact of the atmospheric stability conditions is provided in the first part of the present research [32].

To include the flame length in the fire-spotting model in the form of Formula (2), the maximum travel distance for a spherical firebrand is written, following [25], in the form

$$\ell_{\max} = H_{\max}\left\{\beta_2 \tan(\theta+\omega) + \left[\frac{3}{2}\frac{\rho}{\rho_f}C_d \mathrm{Fr}\right]^{1/2}\right\}, \tag{52}$$

where $\beta_2 = 0.7$ is a correction factor [25] and $\mathrm{Fr} = (U\cos\omega)^2/(gr)$ is the Froude number where r (m) is the firebrand radius. Since, in the general case with both wind and slope, a formula for the tilting angle θ is not yet available, we use the formula provided by Pagni & Peterson [39], which, in our notation, reads $\tan\theta = 1.4U(gL_f)^{-1/2}$. Hence, according to Formula (33), the slope affects the tilting angle through the flame length L_f, such that

$$\tan\theta = 1.4\,\frac{U}{\sqrt{gh_0}\left(1+\phi_{\text{wind}}+\phi_{\text{slope}}\right)^{1/3}}, \tag{53}$$

where h_0 is established in (31); finally, from trigonometric identities, we obtain

$$\tan(\theta+\omega) = \frac{\tan\theta+\tan\omega}{1-\tan\theta\tan\omega}, \quad \cos(\theta+\omega) = \frac{1-\tan\theta\tan\omega}{\left[1+\tan^2\theta\right]^{1/2}}\cos\omega. \tag{54}$$

The maximum landing distance can be represented by a certain p^{th} percentile of the lognormal distribution [28], which is quantified by the parameter z_p such that

$$\ell_{\max} = \mu\exp(z_p\sigma). \tag{55}$$

Thus, from (51,52), and (55), it holds that

$$\sigma = \sigma(\omega) = \frac{1}{z_p}\ln\left\{\frac{U}{\sqrt{gr\,(1+\tan^2\omega)}} + \beta_2\sqrt{\frac{2\rho_f}{3\rho C_d}}\,\frac{1.4U+\sqrt{gh_0(1+\phi_{\text{wind}}+\phi_{\text{slope}})^{2/3}}\tan\omega}{\sqrt{gh_0(1+\phi_{\text{wind}}+\phi_{\text{slope}})^{2/3}}-1.4U\tan\omega}\right\}. \tag{56}$$

To conclude, the phenomenology reproduced by the present parametrisation (56) is that, for an increasing flame length L_f, the parameter σ decreases, while the mode of the lognormal moves towards a larger value of the firebrand's landing distance, with the effect of increasing the probability of generating separate independent fires that are far from the main fire. This effect is studied in the following section through some test cases performed with the wildfire propagation model described and used for simulations in Part 1 [32]; however, the parameter σ is now implemented according to Formulae (56) and (46).

7. Results and discussions

7.1. When the slope rides the bench

We aim to study the effects of flame geometry and slope on fire-spotting. For this purpose, first, we consider a flat terrain, such that we analyse the role of flame geometry only. Later, we discuss the role of slope in comparison with the role of flame geometry.

In particular, based on some experimental measurements of flame length, we simulate sample test cases with a flat terrain and constant wind. The impact of flame geometry on fire-spotting is investigated through the modelling approach described in Part 1 [32], which means that flame length is included in the parametrisation of the lognormal distribution of the firebrand landing distance (50) using Formula (56) for the parameter σ. Briefly, the code used to simulate the fire-front motion is based on the Level-Set Method (LSM) [92], as with other operational fire simulators (see, e.g. [93–95]), while at the post-processing stage, the fire-front is then distributed accordingly to the PDF corresponding to the sum of the random fluctuations due to the turbulent heat transport, i.e. a bi-variate Gaussian density with a diffusion coefficient D, and due to the fire-spotting, i.e. the lognormal (50) with the parametrisation proposed above. Thus, by varying the values of the parameters, different values of σ are obtained.

The results for several formulations are plotted in Fig. 4. This plot shows that, for a sufficiently high fireline intensity, the standard deviation of the firebrand landing distribution σ approaches a constant value, with a very slight dependence on fireline intensity. On the other hand, different formulations of the flame length that also consider environmental factors lead to quite a wide range of possible values of σ.

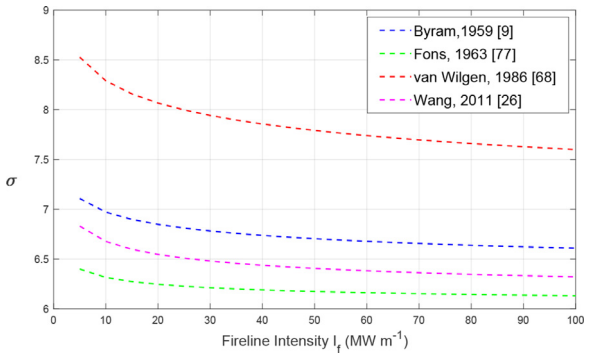

Fig. 4. Parameter σ of the firebrand landing distribution (56) for a flat terrain $\omega = 0$ and constant wind U versus fireline intensity for various empirical formulations of the flame length from Table 1.

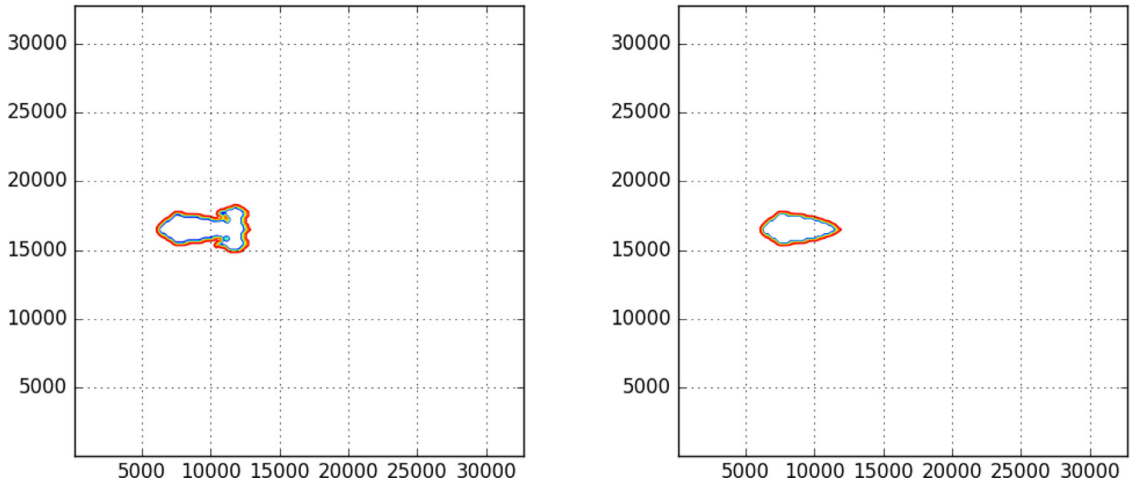

Fig. 5. Fire-front at $t = 119$ min. Left: by including flame length according to (56), such that $\sigma = 7.6$. Right: without considering flame length and $\sigma = 6.4$.

Test 1. Comparison of fire-front propagation with and without flame length We simulate fire spreading with flame length, i.e. parameter σ is computed using Formula (56), and without flame length, i.e. parameter σ is computed as in Part 1 [32]. The wind speed is set as $U = 5.6\,\mathrm{ms}^{-1}$, the fireline intensity as $I_\mathrm{f} = 20\,\mathrm{MW\,m}^{-1}$, and the diffusion coefficient as $D = 0.015\,\mathrm{m}^2\mathrm{s}^{-1}$.

In Part 1 [32], we do not consider flame length, while here, we improve the parameterisation proposed in [28] by including this meso-scale factor. In this example, we study the effect of this improvement by comparing the results of the two parametrisations. In particular, for the considered set of parameters, when the flame length is included, we have, from Formula (56), that $\sigma = 7.6$, and when it is not included, we have that $\sigma = 6.4$. The fire-front simulated using both values is presented in Fig. 5. The results show that the flame length is an influential factor in the fire-spotting model; indeed, in this case, fire-spotting is observed and, due to the merging of the secondary with the primary fires, the resulting front has a more complex shape. The relationship between flame length and fireline intensity may vary due to a plethora of possible system configurations, as shown in Section 5; this explains the variety of the parameters β_0 and β_1 in (2) from the empirical data. Thus, Formula (56) allows us to also adjust the fire-spotting model to different vegetation and environmental conditions.

Test 2. Comparison of fire-front propagation for different flame lengths, as given by different values of β_0: We simulate fire spreading by using the interdependence between flame length and fireline intensity (2)(see Table 1). The other parameters are set as follows: wind speed $U = 4.47\,\mathrm{ms}^{-1}$, fireline intensity $I_\mathrm{f} = 20\,\mathrm{MW\,m}^{-1}$, and diffusion coefficient $D = 0.4238\,\mathrm{m}^2\mathrm{s}^{-1}$.

In this test, we consider the effects of the proposed parametrisation (56) according to various empirical relations between flame length and fireline intensity. Flame length does not affect the parameter μ (51); thus, the value $\mu = 8.419$, obtained by the chosen set-up, is constant and independent of flame length. Different values of σ that correspond to different empirical values of β_0 are collected in Table 2. It turns out that, with a larger flame length L_f, i.e. small σ, the distribution of the

Table 2
Parameters β_0 and σ for fixed $\beta_1 = 2/3$.

References	β_0	σ
Fons, 1963 [77]	0.1270	5.846
Anderson et al. (Douglas-fir slash), 1966 [75]	0.0447	6.191
Wang, 2011 [25]	0.0264	6.415
Butler, 2004 [78]	0.0175	6.615

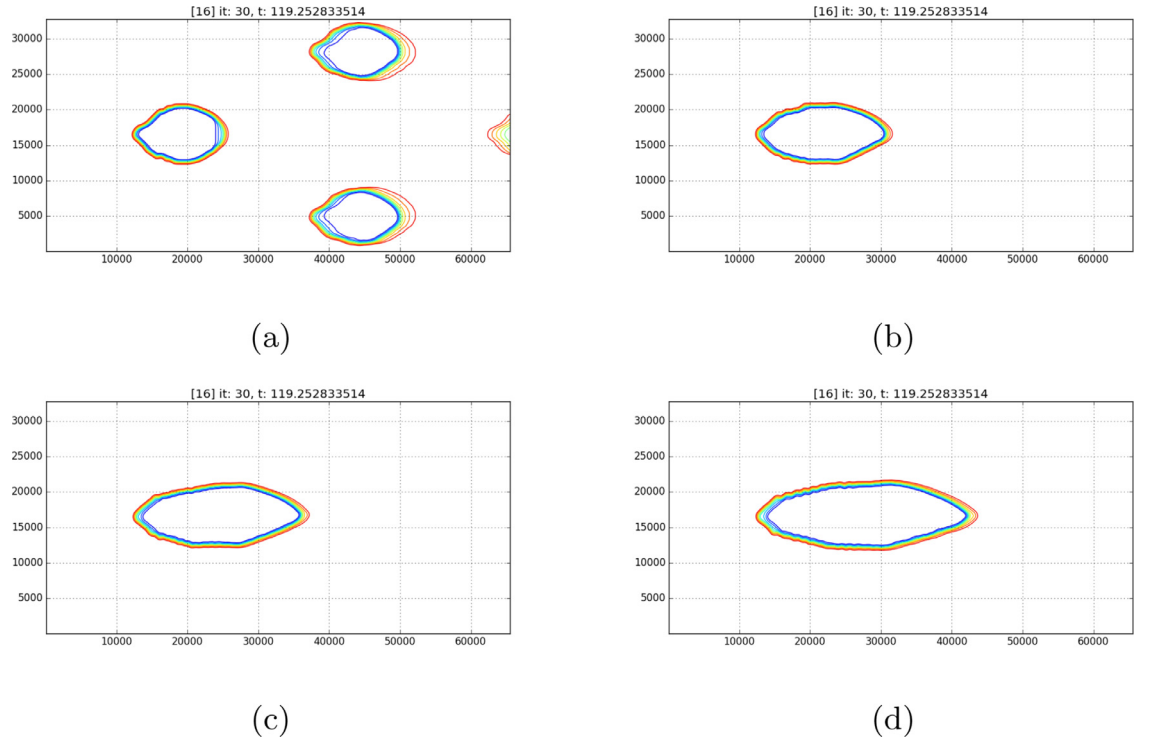

Fig. 6. Fire front at $t = 29$ min simulated by using flame length – fireline intensity formula (2) with $\beta_1 = 2/3$ and various β_0: (a) $\beta_0 = 0.1270$ (Fons, 1963 [77]); (b) $\beta_0 = 0.0447$ (Anderson et al., 1963 [75]); (c) $\beta_0 = 0.0264$ (Wang, 2011 [25]); (d) $\beta_0 = 0.0175$ (Butler, 2004 [78])..

landing distance of the firebrands (50) displays a larger mode that generates long-distance spotting. Hence, the primary fire generates far-away secondary fires that, in turn, rapidly generate further spotting, such that the merging process turns out to be slower than the ignition by fire-spotting. The final pattern results in many independent fires (see Fig. 6a). In contrast, when short-distance spotting occurs, the primary fire rapidly merges with the secondary fires, and a unique cumulative burning zone is observed (see Figs. 6b-d).

Thus, according to the proposed fire-spotting model, a smaller flame length (with the same fire intensity) leads to shorter-distance spotting, usually with a rapid merging of spot-fires. This is consistent with real fires, with many types of fuel with any fireline intensity [16]. These spot fires can generate new fire-spotting, which results in an extremely fast-moving flaming zone (see Fig. 7; the solid line represents the burning area growth in the case of $\beta_0 = 0.1270$, which corresponds to the fire-front given in Fig. 6a).

Test 3. Comparison of fire-front propagation for different flame lengths as given by different values of $\beta_1 \neq 2/3$: We simulate fire spreading using the interdependence between flame length and fireline intensity (2) with fixed β_0 and variable β_1 (see Table 1). The other parameters are set as follows: wind speed $U = 4.47\,\mathrm{ms}^{-1}$, fireline intensity $I_\mathrm{f} = 20\,\mathrm{MWm}^{-1}$ and diffusion coefficient $D = 0.4238\,\mathrm{m}^2\mathrm{s}^{-1}$.

In this test, with reference to Table 1, the values of the empirical parameters β_0 and β_1 and of the corresponding values of σ are reported in Table 3. We highlight the following demonstrative cases:

a. $\beta_1 \approx 1$ corresponds to a linear relation between the flame length and the fireline intensity, as experimentally observed by Clark [80]. A linear relation was, indeed, theoretically established by Albini between flame height and fireline intensity [10], as shown in the derivation of Formula (9) of the present paper. However, from Albini's model, the flame height–fireline intensity relation follows a 2/3 power law (see Formula (11)). Therefore, the linear case remains on an empirical basis only. The burning area at $t = 29$ min is presented in Fig. 8a. The flame described by the parameters $\beta_0 = 0.000722$

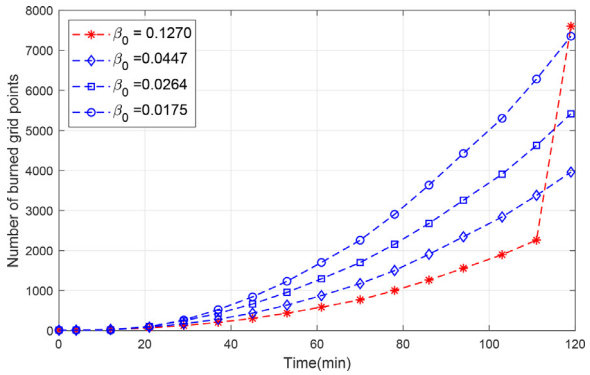

Fig. 7. Burning area with respect to time for various flame length formulations with varying β_0 and fixed $\beta_1 = 2/3$.

Table 3
Empirical parameters of the flame length–fireline intensity interdependence and corresponding values of σ.

References	β_0	β_1	σ
Clark, 1983 [80]	0.000722	0.99	6.115
Weise and Biging, 1996 [17]	0.016	0.7	6.663
Byram, 1959 [9]	0.0775	0.46	6.927

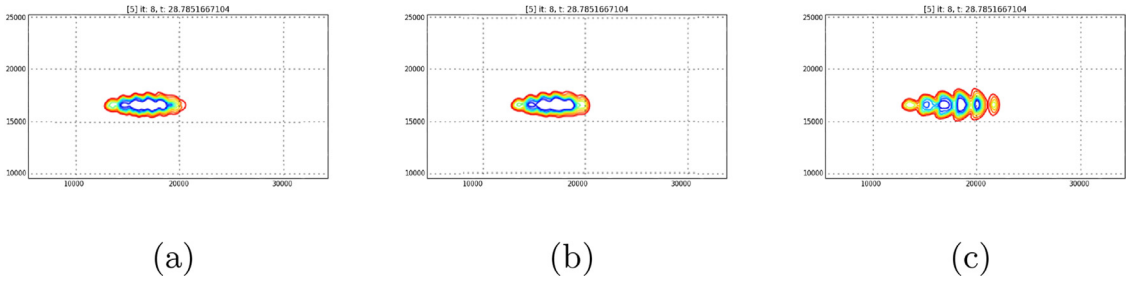

Fig. 8. Fire front at $t = 29$ min simulated by using flame length – fireline intensity formulas proposed in: (a) Clark, 1983 [80], $\beta_0 = 0.016$, $\beta_1 = 0.7$; (b) Weise and Biging, 1996 [17], $\beta_0 = 0.0775$, $\beta_1 = 0.46$; (c) Byram, 1959 [9], $\beta_0 = 0.0775$, $\beta_1 = 0.46$..

and $\beta_1 = 0.99$ generates short-distance spotting characterised by immediate merging. The front propagates faster than the secondary fires ignite; thus, in this case, the impact of fire-spotting in the propagation of the fire front is negligible.

b. The theoretical value for parameter β_1 is expected to be $\beta_1 = 2/3$; thus, we also consider $\beta_1 \approx 2/3$ [17], to determine the effects of small fluctuations in the power-law formula linking flame length and fireline intensity. The result is presented in Fig. 8b. The flame represented by these parameters is similar to the one in the previous case for the chosen value of the fireline intensity. Thus, again, short-distance spotting is observed with fast merging. When the power law is around the theoretical value 2/3, the coefficient β_0 plays an important role because it represents environmental factors for ignition.

c. In this case, we consider the classical power law proposed by Byram [9], i.e. $\beta_1 < 2/3$, which is the most used phenomenological approach. Many recent studies use these empirical parameters to estimate flame length or fireline intensity. The fire front at $t = 29$ min is shown in Fig. 8c. In this case, the effect of secondary fires is more evident, because the travel distance of firebrands exceeds the area swept by the wildfire. This is due to a sufficiently large coefficient β_0; thus, for a fixed fireline intensity, the flame is found to be sufficiently large to produce the secondary fires.

These numerical examples show that flame geometry, particularly flame length, is an important factor for a firebrand landing distribution, in the sense that fluctuations in this parameter may significantly change the behaviour of fire-spotting and, consequently, of front propagation: however, the slope overturns this phenomenology.

7.2. When the slope enters the game

When the propagation of a front occurs along a sloped terrain, the role of the slope cannot be disregarded. Specifically, the effect of the slope on the ROS tends to be stronger on the flame geometry and on the parameter of the firebrands' landing distribution σ (50). This is displayed in the generated patterns of the burned area (see Fig. 9).

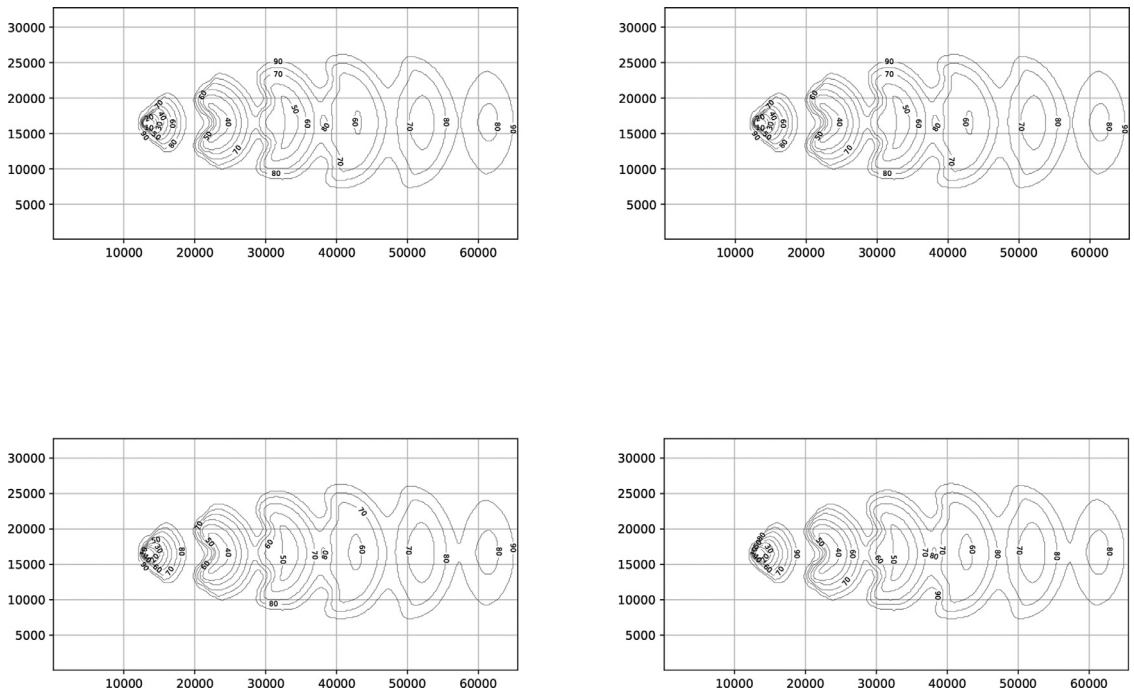

Fig. 9. Fire spreading over a sloping terrain with $\tan\omega = 0, 0.1, 0.5, 0.75$, in clockwise rotation from the top-left, and $U = 10\,\mathrm{ms}^{-1}$. Other parameters are chosen as in Fig. 6(a).

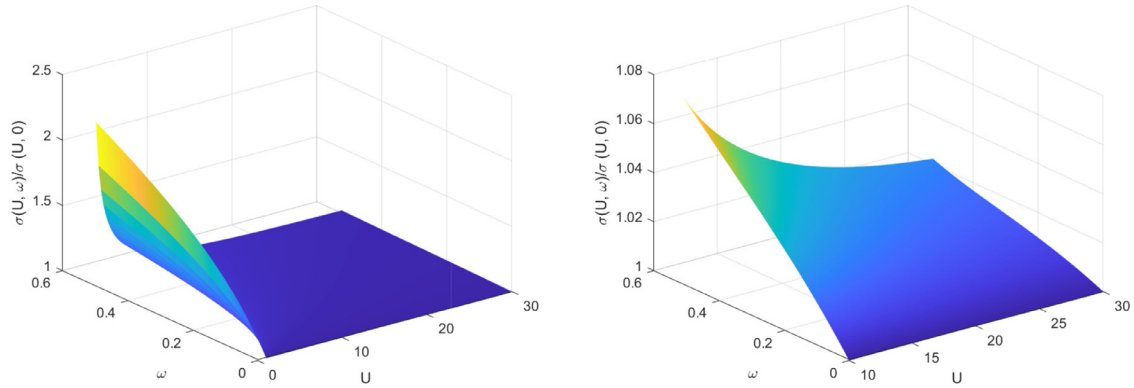

Fig. 10. Variability of parameter σ (56) with respect to the slope ω and the wind U as calculated through the ratio $\sigma(U,\omega)/\sigma(U,0)$.

Indeed, the parameter σ (56), which controls firebrands' landing distance, is almost constant with respect to the slope (see Fig. 10). In contrast, the ROS is strongly accelerated by the slope (see Fig. 11). This difference in the importance of the role of the slope has a remarkable quantitative effect on the resulting burned area, with the final dynamic as follows: Although the slope increases firebrands' landing distance through the contribution of the flame length to the parameter σ, the augmentation of the ROS due to the slope is of such importance that the merging process is sufficiently rapid to cover the generation of secondary fires by fire-spotting.

As a matter of fact, such quantitative difference is an inner part of the formalism, as it emerges from the ratios (29) and (33), and the slope-dependent determination of σ (56): the slope affects the ROS linearly (29), and affects the flame length with the power law 2/3 (33), while it almost does not affect σ (56):

$$\sigma \simeq \frac{1}{z_\mathrm{p}} \ln\left\{ \frac{U}{\sqrt{gr\left(1+\omega^2\right)}} + \beta_2 \sqrt{\frac{2\rho_\mathrm{f}}{3\rho\, C_\mathrm{d}}}\, \frac{\omega+\Phi}{1-\Phi\omega} \right\}, \tag{57}$$

where $\Phi = 1.4\,U/\sqrt{gh_0(1+\phi_\mathrm{wind}+5.275\,\omega^2/\beta^{0.3})^{2/3}}$ and the approximation $\sqrt{\phi_\mathrm{slope}} \propto \tan\omega \simeq \omega$ has been used.

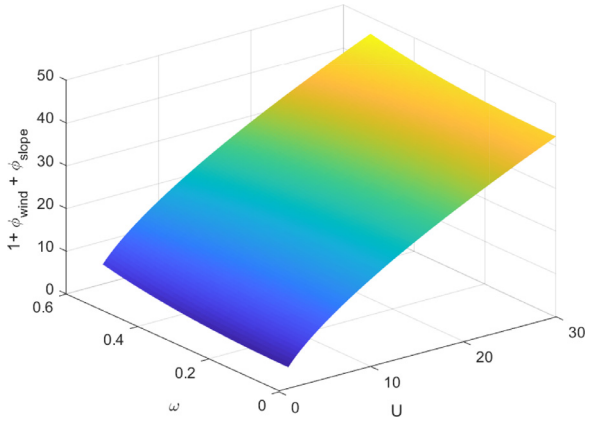

Fig. 11. Variability of the ROS with respect to the slope ω and the wind U as calculated through the ratio (29).

8. Conclusions

In this study, we have analysed the role of meso-scopic features in the propagation of wildfires. Specifically, we have considered flame geometry and terrain slope.

The $2/3$ power-law relationship between flame length and fireline intensity is theoretically established based on the energy conservation principle and the energy flow rate in the convection column above the fireline, considering wind and slope. This new formulation refines the previous results by Albini [10] and Nelson Jr. and co-authors [5].

It is well established by experiments that flame length is related to fireline intensity while, because of a trigonometric relation, flame length is linearly proportional to flame height. The trigonometric factor of proportionality turns out to be independent of fireline intensity, while its variability is mainly due to wind and slope. The proposed formula allows for an estimation of the influence of some ambient factors on flame geometry using definition (36). Therefore, for realistic tests with the same (dimensionally correct) power-law factor, smaller values of the proportionality coefficient represent a higher ambient temperature or vegetation with higher specific heat. Hence, for different types of fuel, flame length relates to fireline intensity through different coefficients of proportionality. Thus, the proposed formula allows a specification of the fire-spotting model in accordance with the type of fuel in each particular case.

The proposed fire-spotting model is based on a lognormal distribution of firebrands' landing distance, and depends on two parameters: μ and σ. Both parameters depend on ambient factors, such as wind speed and air temperature. Parameter μ also considers the atmospheric stability conditions. As shown in the first part of the present study [32], the boundary layer depth slightly affects the fire-spotting itself; however, it is more significant for turbulence because it affects the propagation of the main fire. Parameter σ is extended here to account for, apart from the wind velocity, the flame geometry and the slope. Note that the vegetation feeds the fire by affecting the fireline intensity and, consequently, the flame length. Thus, by adding the flame length, we include the specified surround vegetation factors in the model, i.e. we adjust the model to various local conditions. In other words, depending on the flame length, different scenarios can be modelled.

This flexibility meets the requirements for the validation of wildfire spread models that, to cover a sufficient range of conditions, must include a certain level of variability in the values of the main parameters, such as wind speed and fuel moisture content [35]. However, we remind the reader of the large uncertainties that still affect the simulations of fire spreading; thus, validation relies more on probabilistic forecasting than on a single deterministic prediction [96]. In this sense, the flexibility of the present formulation allows for an input distribution of the desired parameters.

Numerical examples show intriguing patterns. Indeed, on flat terrain, flame length is a significant factor in the fire-spotting model, due to its effects on the distribution of firebrands' landing distance. Flame geometry changes a firebrand's travel distance and, in terms of the proposed model, the parameter σ of the lognormal distribution, such that the following situations can be observed:

1. No fire-spotting: when a firebrand travel distance is insufficient to produce an independent secondary fire. Usually, this happens when the flame length is not sufficiently large.
2. Merging of secondary fires: when the propagation of the main fire front is more rapid than the generation of secondary fires. In this case, fire-spotting still occurs, but the main front catches up to the secondary fires.
3. Fire-spotting: when a flame is large enough to generate firebrands that can travel a long distance. Each secondary fire later produces new secondary fires; thus, the fire-front propagation speed increases rapidly, a larger area is burned, and the risk that the fire passes over obstacles and fire-safety zones is much higher.

However, when the propagation occurs on sloped terrain, the slope enhances the ROS sufficiently for the speed of the merging process among independent fires to remove the generation of fire-spotting ignited fires. This result follows from the whole formulation derived here.

Thus, we summarise the findings of our study by stating that the two meso-scopic features considered here have the following roles: increasing the flame length increases firebrands' landing distance and then independent fires, generated by fire-spotting, emerge; however, the presence of a slope increases the ROS by causing a fast merging among the independent fires.

We end by reporting that the simulations were performed using the code LSFire+, programmed in C and Fortran, in which the model proposed here acts as a post-processing routine at each time step in an LSM code [97]. The simulations were run on the cluster HYPATIA at BCAM, Bilbao, using OpenMP memory parallelism shared in 24 cores inside 395 of an Intel(R) Xeon(R) CPU E5-2680 v3 2.50GHz node with 128GB RAM. Running the code for 45 simulated minutes required approximatively 140 minutes of physical time. The code LSFire+ is freely available at the official git repository of BCAM at:
https://gitlab.bcamath.org/atrucchia/randomfront-wrfsfire-lsfire.

Acknowledgements

This research is supported by the Basque Government through the BERC 2014–2017 and the BERC 2018–2021 programs, the Spanish Ministry of Economy and Competitiveness MINECO through the BCAM Severo Ochoa excellence accreditations SEV-2013-0323 and SEV-2017-0718 and through the projects MTM2016-76016-R and PID2019-107685RB-I00, and by the PhD grant "La Caixa 2014".

References

[1] A.C. Fernandez-Pello, Wildland fire spot ignition by sparks and firebrands, Fire Safety J. 91 (2017) 2–10.
[2] D. Morvan, V. Tauleigne, J.L. Dupuy, Flame geometry and surface to crown fire transition during the propagation of a Line fire through a Mediterranean shrub, in: D.X. Viegas (Ed.), Forest Fire Research & Wildland Fire Safety, Millpress, Rotterdam, 2002.
[3] https://www.nwcg.gov/publications/training-courses/s-290.
[4] J.L. Rossi, K. Chetehouna, A. Collin, B. Moretti, J.H. Balbi, Simplified flame models and prediction of the thermal radiation emitted by a flame front in an outdoor fire, Combust. Sci. Technol. 182 (2010) 1457–1477.
[5] R.M. Nelson Jr, B.W. Butler, D.R. Weise, Entrainment regimes and flame characteristics of wildland fires, Int. J. Wildland Fire 21 (2012) 127–140.
[6] M.J. Campbell, P.E. Dennison, B.W. Butler, Safe separation distance score: a new metric for evaluating wildland firefighter safety zones using lidar, Int. J. Geogr. Inf. Sci. 31(7) (2016) 1448–1466.
[7] A.A.G. Wilson, I.S. Ferguson, Predicting the probability of house survival during bushfires, J. Environ. Manage. 23 (1986) 259–270.
[8] M.E. Alexander, M.G. Cruz, Interdependencies between flame length and fireline intensity in predicting crown fire initiation and crown scorch height, Int. J. Wildland Fire 21 (2012) 95–113.
[9] G.M. Byram, Combustion of forest fuels, in: K.P. Davis (Ed.), Forest Fire: Control and Use, McGraw Hill, New York, 1959, pp. 61–89.
[10] F.A. Albini, A model for the wind-blown flame from a line fire, Combust. Flame 43 (1981) 155–174.
[11] T. Marcelli, J.H. Balbi, B. Moretti, J.L. Rossi, F.J. Chatelon, Flame height model of a spreading surface fire, in: Proceedings of the 7th Mediterranean Combustion Symposium (MCS7), Cagliari, Italy, 2011. Art. No. FE-10. ISBN 978-88-88104-12-6
[12] L. Ferragut, M.I. Asensio, J.M. Cascón, D. Prieto, A wildland fire physical model well suited to data assimilation, Pure Appl. Geophys. 172 (2015) 121–139.
[13] R.M. Nelson Jr, Byram's energy criterion for wildland fires: units and equations, Research Note INT-415, Intermountain Research Station, 1993.
[14] A.L. Sullivan, Convective Froude number and Byram's energy criterion of Australian experimental grassland fires, Proc. Combust. Inst. 31 (2007) 2557–2564.
[15] A.L. Sullivan, Inside the inferno: fundamental processes of wildland fire behaviour. Part 1: combustion chemistry and heat release, Curr. Forestry Rep. 3 (2017) 132–149.
[16] A.L. Sullivan, Inside the inferno: fundamental processes of wildland fire behaviour. Part 2: heat transfer and interaction, Curr. Forestry Rep. 3 (2017) 150–171.
[17] D.R. Weise, G.S. Biging, Effects of wind velocity and slope on flame properties, Can. J. For. Res 26 (1996) 1849–1858.
[18] D.R. Weise, T.H. Fletcher, S.M.X. Zhou, L. Sun, Fire spread in chaparral: comparison of data with flame-mass loss relationships, Eigth International Symposium on Scale Modeling (ISSM-8), Portland, Oregon, USA, September 12–14, 2017.
[19] D.R. Weise, T.H. Fletcher, W. Cole, S. Mahalingam, X. Zhou, L. Sun, J. Li, Fire behavior in chaparralevaluating flame models with laboratory data, Combust. Flame 191 (2018) 500–512.
[20] G.M. Byram, Forest fire behavior, in: K.P. Davis (Ed.), Forest Fire: Control and Use, McGraw Hill, New York, 1959, pp. 90–123.
[21] R.C. Rothermel, A Mathematical Model for Predicting Fire Spread in Wildland Fires, Research Paper INT-115, USDA Forest Service, Intermountain Forest and Range Experiment Station, Ogden, Utah 84401, 1972. Available at: http://www.treesearch.fs.fed.us/pubs/32533
[22] P.L. Andrews, The Rothermel Surface Fire Spread Model and Associated Developments: A Comprehensive Explanation, Gen. Tech. Rep., Fort Collins, CO: U.S. Department of Agriculture, Forest Service, Rocky Mountain Research Station, 2018. RMRS-GTR-371
[23] E. Koo, P.J. Pagni, D.R. Weise, J.P. Woycheese, Firebrands and spotting ignition in large-scale fires, Int. J. Wildland Fire 19 (2010) 818–843.
[24] J. Martin, T. Hillen, The spotting distribution of wildfires, Appl. Sci. 6 (6) (2016) 177–210.
[25] H.-H. Wang, Analysis on downwind distribution of firebrands sourced from a wildland fire, Fire Technol. 47 (2) (2011) 321–340.
[26] I. Kaur, G. Pagnini, Fire-spotting modelling and parametrisation for wild-land fires, in: S. Sauvage, J.M. Sánchez-Pérez, A.E. Rizzoli (Eds.), Proceedings of the 8th International Congress on Environmental Modelling and Software (iEMSs2016); Toulouse, France, 10–14 July (2016), 2016, pp. 384–391. ISBN: 978-88-9035-745-9
[27] G. Pagnini, A. Mentrelli, Modelling wildland fire propagation by tracking random fronts, Nat. Hazards Earth Syst. Sci. 14 (2014) 2249–2263.
[28] I. Kaur, A. Mentrelli, F. Bosseur, J.-B. Filippi, G. Pagnini, Turbulence and fire-spotting effects into wild-land fire simulators, Commun. Nonlinear Sci. Numer. Simul. 39 (2016) 300–320.
[29] A. Trucchia, V.N. Egorova, A. Butenko, I. Kaur, G. Pagnini, Randomfront 2.3: a physical parametrisation of fire spotting for operational fire spread models - implementation in WRF-SFIRE and response analysis with LSFire+, Geosci. Model Dev. 12 (2019) 69–87.
[30] A. Trucchia, V.N. Egorova, G. Pagnini, M.C. Rochoux, On the merits of sparse surrogates for global sensitivity analysis of multi-scale nonlinear problems: application to turbulence and fire-spotting model in wildland fire simulators, Commun. Nonlinear Sci. Numer. Simul. 73 (2019) 120145.
[31] M.I. Asensio, L. Ferragut, D. Alvarez, P.L. P, J.M. Cascón, D. Prieto, G. Pagnini, PhyFire: an online GIS-integrated wildfire spread simulation tool based on a semiphysical model, in: M.I. Asensio, A. Oliver, J. Sarrate (Eds.), Applied Mathematics for Environmental Problems, ICIAM 2019 SEMA SIMAI Springer Series, volume 6, Springer Nature Switzerland AG, 2021, pp. 1–20.
[32] V.N. Egorova, A. Trucchia, G. Pagnini, Fire-spotting generated fires. Part I: the role of atmospheric stability, Appl. Math. Model. 84 (2020) 590–609.
[33] V.N. Egorova, A. Trucchia, G. Pagnini, Physical parametrisation of fire-spotting for operational wildfire simulators, in: M.I. Asensio, A. Oliver, J. Sarrate (Eds.), Applied Mathematics for Environmental Problems, ICIAM 2019 SEMA SIMAI Springer Series, volume 6, Springer Nature Switzerland AG, 2021, pp. 21–38.

[34] A.L. Sullivan, M.G. Cruz, Small-scale flame dynamics provide limited insight into wildfire behavior, Proc. Natl. Acad. Sci. U.S.A. 112 (31) (2015) E4164.
[35] D. Morvan, Validation of Wildfire Spread Models, in: S.L. Manzello (Ed.), Encyclopedia of Wildfires and Wildland-Urban Interface (WUI) Fires, Springer Nature, Switzerland AG, 2019.
[36] F.A. Williams, Scaling mass fires, Fire Res. Abstr. Rev. 11 (1969) 1–22.
[37] H.C. Hottel, Fire modeling, in: W.G. Berl (Ed.), International Symposium on the Use of Models in Fire Research, National Research Council, The National Academies Press, Washington, DC, 1961, pp. 32–47. ISBN 978-0-309-34048-9; https://doi.org/10.17226/20284
[38] J.G. Quintiere, Scaling applications in fire research, Fire Saf. J. 15 (1) (1989) 3–29.
[39] P.J. Pagni, T.G. Peterson, Flame spread through porous fuels, Symp. Combust. Proc. 14 (1973) 1099–1107.
[40] B.A. Adam, N.K. Akafuah, M.A. Finney, J.M. Forthofer, K. Saito, A study of flame spread in engineered cardboard fuelbeds. Part II: Scaling law approach, in: Progress in Scale Modeling, volume II, Springer, Berlin/Heidelberg, Germany, 2014, pp. 85–95.
[41] D.B. Spalding, The art of partial modelling, Symp. Combust. Proc. 9 (1963) 833–843.
[42] M.A. Delichatsios, Air entrainment into buoyant jet flames and pool fires, Combust. Flame 70 (1) (1987) 33–46.
[43] W.M. Pitts, Wind effects on fires, Prog. Energy Combust. Sci. 17 (2) (1991) 83–134.
[44] R.E. Martin, M.A. Finney, D.M. Molina, D.B. Sapsis, S.L. Stephens, J.H. Scott, D.R. Weise, Dimensional analysis of flame angles versus wind speed, in: P.L. Andrews, D.F. Potts (Eds.), Proceedings of the 11th Conference on Fire and Forest Meteorology, Society of American Foresters, Bethesda, MD., Missoula, Montana, 1991, pp. 212–217.
[45] M.A. Finney, J.D. Cohen, J.M. Forthofer, S.S. McAllister, M.J. Gollner, D.J. Gorham, K. Saito, N.K. Akafuah, B.A. Adam, J.D. English, Role of buoyant flame dynamics in wildfire spread, Proc. Natl. Acad. Sci. U.S.A. 112 (32) (2015) 9833–9838.
[46] J.C. Yang, Dimensional analysis on forest fuel bed fire spread, Can. J. For. Res. 48 (1) (2018) 105–110.
[47] Y. Lin, M.A. Delichatsios, X. Zhang, L. Hu, Experimental study and physical analysis of flame geometry in pool fires under relatively strong cross flows, Combust. Flame 205 (2019) 422–433.
[48] A.L. Sullivan, P.F. Ellis, I.K. Knight, A review of radiant heat flux models used in bushfire applications, Int. J. Wildland Fire 12 (1) (2003) 101–110.
[49] D. Frankman, B.W. Webb, B.W. Butler, D. Jimenez, J.M. Forthofer, P. Sopko, K.S. Shannon, J.K. Hiers, R.D. Ottmar, Measurements of convective and radiative heating in wildland fires, Int. J. Wildland Fire 22 (2) (2013) 157–167.
[50] J.E. Hilton, C. Miller, A.L. Sullivan, A power series formulation for two-dimensional wildfire shapes, Int. J. Wildland Fire 25 (9) (2016) 970–979.
[51] P.M. Fernandes, M.G. Cruz, Plant flammability experiments offer limited insight into vegetation-fire dynamics interactions, New Phytol. 194 (3) (2012) 606–609.
[52] F. Rodríguez y Silva, M. Guijarro, J. Madrigal, E. Jiménez, J.R. Molina, C. Hernando, R.A.V. Vélez, J.A. Vega, Assessment of crown fire initiation and spread models in mediterranean conifer forests by using data from field and laboratory experiments, For. Syst. 26 (2017) 2.
[53] Y. Pérez, E. Pastor, A. Àgueda, E. Planas, Effect of wind and slope when scaling the forest fires rate of spread of laboratory experiments, Fire Technol. 47 (2) (2011) 475–489.
[54] J.M. Fox, G.M. Whitesides, Warning signals for eruptive events in spreading fires, Proc. Natl. Acad. Sci. U.S.A. 112 (8) (2015) 2378–2383.
[55] J.M. Fox, G.M. Whitesides, Reply to sullivan and cruz: defense of a simplified physical model, Proc. Natl. Acad. Sci. U.S.A. 112 (31) (2015) E4165.
[56] J.H. Balbi, F.J. Chatelon, D. Morvan, J.L. Rossi, T. Marcelli, F. Morandini, A convectiveradiative propagation model for wildland fires, Int. J. Wildland Fire 29 (8) (2020) 723–738.
[57] L.H. Hu, C. Kuang, X.P. Zhong, Research on pool fire behaviors in wind - State of the art and future challenges, in: J. Chao, N.A. Liu, V. Molkov, P. Sunderland, F. Tamanini, J. Torero (Eds.), Proceedings of the Eighth International Seminar on Fire and Explosion Hazards (ISFEH8), Published by USTC Press, Hefei, China, 2016, pp. 12–21, doi:10.20285/c.sklfs.8thISFEH.002.
[58] M.G. Cruz, M.E. Alexander, Flame Dimensions, in: S.L. Manzello (Ed.), Encyclopedia of Wildfires and Wildland-Urban Interface (WUI) Fires, Springer Nature, Switzerland AG, 2019.
[59] J.H. Balbi, J.L. Rossi, T. Marcelli, P.A. Santoni, A 3D physical real-time model of surface fires across fuel beds, Combust. Sci. Technol. 179 (2007) 2511–2537.
[60] J.H. Balbi, F. Morandini, X. Silvani, J.B. Filippi, F. Rinieri, A physical model for wildland fires, Combust. Flame 156 (2009) 2217–2230.
[61] P.-A. Santoni, J.-B. Filippi, J.-H. Balbi, F. Bosseur, Wildland fire behaviour case studies and fuel models for landscape-scale fire modeling, J. Combust. 2011 (2011) 613424.
[62] M.E. Alexander, Calculating and interpreting forest fire intensities, Can. J. Bot. 60 (1982) 349–357.
[63] M.E. Alexander, M.G. Cruz, Fireline Intensity, in: S.L. Manzello (Ed.), Encyclopedia of Wildfires and Wildland-Urban Interface (WUI) Fires, Springer Nature, Switzerland AG, 2019.
[64] T. Barboni, F. Morandini, L. Rossi, T. Molinier, P. Santoni, Relationship between flame length and fireline intensity obtained by calorimetry at laboratory scale, Combust. Sci. Technol. 184 (2) (2012) 186–204.
[65] T. Maynard, M. Princevac, D.R. Weise, A study of the flow field surrounding interacting line fires, J. Combust. 2016 (Article ID 6927482) (2016).
[66] J.M. Johnston, M.J. Wooster, R. Paugam, X. Wang, T.J. Lynham, L.M. Johnston, Direct estimation of Byram's fire intensity from infrared remote sensing imagery, Int. J. Wildland Fire 26 (2017) 668–684.
[67] P.M. Fernandes, W.R. Catchpole, F.C. Rego, Shrubland fire behaviour modelling with microplot data, Can. J. For. Res 30 (2000) 889–899.
[68] B.W. van Wilgen, A simple relationship for estimating the intensity of fires in natural vegetation, S. African J. Bot. 52 (1986) 384–385.
[69] R.M. Nelson Jr, C.W. Adkins, Flame characteristics of wind-driven surface fires, Can. J. For. Res. 16 (1986) 1293–1300.
[70] J.A. Vega, P. Cuinas, T. Fonturbel, P. Perez-Gorostiaga, C. Fernandez, Predicting fire behaviour in Galician (NW Spain) shrubland fuel complexes, in: Proceedings of 3rd International Conference on Forest Fire Research and 14th Conference on Fire and Forest Meteorology, Volume II, 1998, pp. 713–728.
[71] M. Newman, Toward a common language for aerial delivery mechanics, Fire Manage. Notes 35 (1) (1974) 18–19.
[72] R.M. Nelson Jr, Flame characteristics for fires in southern fuels, USDA Forest Service, Southeastern Forest Experiment Station, Research Paper SE-205 (1980).
[73] P.M. Fernandes, H.S. Botelho, F. Rego, C. Loureiro, Empirical modelling of surface fire behaviour in maritime pine stands, Int. J. Wildland Fire 18 (2009) 698–710.
[74] W.R. Catchpole, R.A. Bradstock, J. Choate, L.G. Fogarty, N. Gellie, G. McCarthy, W.L. McCaw, J.B. Marsden-Smedley, G. Pearce, Cooperative development of equations for heathland fire behaviour, in: Proceedings of 3rd International Conference on Forest Fire Research and 14th Conference on Fire and Forest Meteorology, Volume II, 1998, pp. 631–645.
[75] H.E. Anderson, A.P. Brackebusch, R.W. Mutch, R.C. Rothermel, Mechanisms of fire spread research progress report 2, USDA Forest Service, Intermountain Forest and Range Experiment Station, Research Paper INT-28. (Ogden, UT) (1966).
[76] P. Thomas, The size of flames from natural fires, Symp. Combust. Proc. 9 (1963) 844–859.
[77] W.L. Fons, H.B. Clements, P.M. George, Scale effects on propagation rate of laboratory crib fires, Symp. Combust. Proc. 9 (1963) 860–866.
[78] B.W. Butler, M.A. Finney, P.L. Andrews, F.A. Albini, A radiation-driven model of crown fire spread, Can. J. For. Res. 34 (2004) 1588–1599.
[79] N.D. Burrows, Experimental Development of a Fire Management Model for Jarrah (Eucalyptus Marginata Donn ex Sm.) forest, Australian National University, Canberra, 1994 Ph.D. thesis.
[80] R.G. Clark, Threshold Requirements for Fire Spread in Grassland Fuels, Texas Tech University, Lubbock, 1983 Ph.D. thesis.
[81] Y. Brunet, U. Kyaw Tha Paw, L. Prevot, Using the radiative surface temperature in energy budget studies over plant canopies, in: Proc. Fifth Int. Colloquium on Physical Measurements and Signatures in Remote Sensing, European Space Agency, Courchevel, France, 1991, pp. 557–560.
[82] W. Brutsaert, M. Sugita, Sensible heat transfer parameterization for surfaces with anisothermal dense vegetation, J. Atmos. Sci. 53 (2) (1996) 209–216.
[83] J. Yang, Y. Wang, D.R. Miller, Estimating air temperature profiles in forest canopy using empirical models and Landsat data, For. Sci. 53 (2007) 93–99.
[84] E. Inoue, On the turbulent structure of airflow within corn canopies, J. Meteorol. Soc. Jpn. 41 (1963) 317–326.

[85] R.M. Cionco, A mathematical model for airflow in a vegetative canopy, J. Appl. Meteorol. 4 (1965) 517–522.
[86] Y. Brunet, Turbulent flow in plant canopies: historical perspective and overview, Boundary-Layer Meteorol. 177 (2020) 315–364.
[87] R.M. Nelson Jr, Byram's Energy Criterion for Wildland Fires: Units and Equations, Research Note INT-415, Intermountain Research Station, Forest Service, 1993.
[88] F. Nmira, J.L. Consalvi, P. Boulet, B. Porterie, Numerical study of wind effects on the characteristics of flames from non-propagating vegetation fires, Fire Safety J. 45(2) (2010) 129–141.
[89] A.L. Sullivan, Convective Froude number and Byram's energy criterion of Australian experimental grassland fires, Proc. Combust. Inst. 31 (2007) 2557–2564.
[90] N.M. Vaillant, A.A. Ager, J. Anderson, L. Miller, ArcFuels User Guide and Tutorial: for use with ArcGIS 9, Gen. Tech. Rep. PNW-GTR-877, U.S. Department of Agriculture, Forest Service, Pacific Northwest Research Station, 2013.
[91] M. Sofiev, T. Ermakova, R. Vankevich, Evaluation of the smoke-injection height from wild-land fires using remote-sensing data, Atmos. Chem. Phys. 12 (4) (2012) 1995–2006.
[92] J.A. Sethian, P. Smereka, Level set methods for fluid interfaces, Ann. Rev. Fluid Mech. 35 (2003) 341–372.
[93] V. Mallet, D.E. Keyes, F.E. Fendell, Modeling wildland fire propagation with level set methods, Comput. Math. Appl. 57 (2009) 1089–1101.
[94] J. Mandel, J.D. Beezley, A.K. Kochanski, Coupled atmosphere-wildland fire modeling with WRF 3.3 and SFIRE 2011, Geosci. Model Dev. 4 (2011) 591–610.
[95] A. Alessandri, P. Bagnerini, M. Gaggero, L. Mantelli, Parameter estimation of fire propagation models using level set methods, Appl. Math. Model. 92 (2021) 731–747.
[96] F. Allaire, V. Mallet, J.-B. Filippi, Novel method for a posteriori uncertainty quantification in wildland fire spread simulation, Appl. Math. Model. 90 (2021) 527–546.
[97] K.T. Chu, M. Prodanović, Level Set Method Library (LSMLIB), 2009. http://ktchu.serendipityresearch.org/software/lsmlib/